Chemistry and Physics of the Novel Molecular-Based Compound Exhibiting a Spontaneous Magnetization Below T_c = 14 K, MnCu(obbz)·1H_2O (obbz = Oxamidobis(benzoato)). Comparison with the Antiferromagnet MnCu(obbz)·5H_2O. Crystal Structure and Magnetic Properties of NiCu(obbz)·6H_2O

Keitaro Nakatani,[†] Jean Yves Carriat,[†] Yves Journaux,[†] Olivier Kahn,*[,†] Francisco Lloret,[†,‡] Jean Pierre Renard,[§] Yu Pei,[†] Jorunn Sletten,[∥] and Michel Verdaguer[†,⊥]

Contribution from the Laboratoire de Spectrochimie des Elêments de Transition, UA No. 420, Institut d'Electronique Fondamentale, UA No. 022, and Laboratoire d'Utilisation du Rayonnement Synchrotron, Universitê de Paris-Sud, 91405 Orsay, France, and Department of Chemistry, University of Bergen, 5007 Bergen, Norway. *Received November 30, 1988*

Abstract: The three compounds MnCu(obbz)·5H_2O, MnCu(obbz)·1H_2O, and NiCu(obbz)·6H_2O, hereafter abbreviated as MnCu·5H_2O, MnCu·1H_2O, and NiCu respectively, have been synthesized. obbz stands for oxamidobis(benzoato). The crystal structure of NiCu has been determined. NiCu crystallizes in the monoclinic system, space group $P2_1/n$, with a = 7.764 (1) Å, b = 12.559 (3) Å, c = 20.083 (3) Å, β = 97.56°, and Z = 4. The structure consists of isolated heterodinuclear units with octahedral Ni(II) and square-planar Cu(II) ions bridged by an oxamido group. NiCu is not isomorphous to MnCu·5H_2O or to MnCu·1H_2O, neither of which has been obtained in the form of single crystals suitable for X-ray work. To get information on their structure, we have studied their XANES and EXAFS spectra at both Mn and Cu edges, as well as their powder X-ray patterns. MnCu·5H_2O and MnCu·1H_2O have very similar structures, with four noncoordinated water molecules in the former compound. Cu(II) is in elongated tetragonal surroundings and Mn(II) in octahedral surroundings. The radius of the first shell around Mn(II) is equal to 2.17 (2) Å for MnCu·5H_2O and 2.16 (2) Å for MnCu·1H_2O. Those data are consistent with the following structure: Mn(II) would be surrounded by six oxygen atoms; two of these atoms MnCu·1H_2O belong to an oxamido group, one to a carboxylato group, and one to a water molecule in the equatorial plane; the oxygen atoms in the apical positions would belong to other carboxylato groups, forming a two- or three-dimensional network. The magnetic properties of NiCu were studied in the 4.2–300 K temperature range. They are typical of an isolated heteropair with a doublet–quartet energy gap $3J/2$ equal to −156 (3) cm^{-1}. The magnetic properties of MnCu·5H_2O, down to 4 K, are characteristics of alternating bimetallic chains with a minimum in the $\chi_M T$ versus T plot, χ_M being the molar magnetic susceptibility per MnCu unit and T the temperature. At 2.3 K, $\chi_M T$ for MnCu·5H_2O shows a sharp maximum due to a three-dimensional antiferromagnetic ordering. In contrast, the $\chi_M T$ versus T plot for MnCu·1H_2O diverges when T approaches the critical temperature T_c = 14 K. Below T_c, MnCu·1H_2O exhibits a spontaneous magnetization. The field dependences of the magnetization M for MnCu·5H_2O and MnCu·1H_2O have been compared. For both compounds, the saturation magnetization corresponds to a S = 2 resulting spin per MnCu unit. Moreover, MnCu·1H_2O at 4.2 K exhibits an $M = f(H)$ hysteresis loop characteristic of a soft magnet. The powder X-band EPR spectra of MnCu·5H_2O and MnCu·1H_2O have been recorded at various temperatures down to 15 K. The comparison of the line widths suggests that the mechanism of the magnetic ordering observed for MnCu·1H_2O is of exchange interaction nature rather than of dipolar nature. The perspectives in the field of the molecular-based ferromagnets are discussed.

Several groups are presently working on the design of molecular-based ferromagnets,[1-9] and the first compounds of this kind have recently been reported. To the best of our knowledge, so far, three molecular-based systems exhibiting a ferromagnetic transition have been fully characterized from both structural and magnetic viewpoints. These systems are as follows: (i) [Fe(Me_5Cp)$_2$](TCNE) with Me_5Cp = pentamethylcyclopentadienyl and TCNE = tetracyanoethylene.[10] T_c is equal to 4.8 K. (ii) MnCu(pbaOH)(H_2O)$_3$ with pbaOH = 2-hydroxy-1,3-propylenebis(oxamato).[11] T_c is then equal to 4.6 K. (iii) Mn(hfa)$_2$(NITMe) with hfa = hexafluoroacetylacetonato and NITiPr = 2-isopropyl-4,4,5,5-tetramethyl-4,5-dihydro-1*H*-imidazolyl-1-oxyl 3-oxide. T_c is reported as 7.8 K. Recently, in a preliminary communication, we reported on a novel molecular-based ferromagnet ordering at 14 K, namely, MnCu(obbz)·1H_2O with obbz = oxamidobis(benzoato).[13] This paper is devoted to a thorough study of this compound and to a comparison of its physical properties with those of its precursor MnCu(obbz)·5H_2O, which orders antiferromagnetically.

[†] Laboratoire de Spectrochimie des Eléments de Transition, Université de Paris-Sud.
[‡] Permanent address: University of Valencia.
[§] Institut d'Electronique Fondamentale, Université de Paris-Sud.
[∥] University of Bergen.
[⊥] Laboratorie d'Utilisation du Rayonnement Synchrotron, Université de Paris-Sud.

(1) Miller, J. S.; Epstein, A. J.; Reiff, W. M. *Chem. Rev.* **1988**,, *88*, 201; *Acc. Chem. Res.* **1988**, *21*, 114; *Science* **1988**, *240*, 40.
(2) Kahn, O. *Struct. Bonding (Berlin)* **1987**, *68*, 89; *NATO ASI Ser. B* **1987**, *168*, 93.
(3) Korshak, Yu. V.; Medvedeva, T. V.; Ovchinnikov, A. A.; Spector, V. N. *Nature* **1987**, *326*, 370.
(4) Fukutome, H.; Takahashi, A.; Ozaki, M. *Chem. Phys. Lett.* **1987**, *133*, 34.
(5) LePage, T. J.; Breslow, R. *J. Am. Chem. Soc.* **1987**, *109*, 6412.
(6) Torrance, J. B.; Oostra, S.; Nazzal, A. *Synth. Met.* **1987**, *19*, 708.
(7) Sugawara, T.; Bandow, S.; Kimura, K.; Iwamura, H.; Itoh, K. *J. Am. Chem. Soc.* **1986**, *108*, 368.
(8) Izuoka, A.; Murata, S.; Sugawara, T.; Iwamura, H. *J. Am. Chem. Soc.* **1987**, *109*, 2631.
(9) Miller, J. S.; Epstein, A. J. *J. Am. Chem. Soc.* **1987**, *109*, 3850.
(10) Miller, J. S.; Calabrese, J. C.; Rommelmann, H.; Chittipeddi, S. R.; Zhang, J. H.; Reiff, W. M.; Epstein, A. J. *J. Am. Chem. Soc.* **1987**, *109*, 769.
(11) Kahn, O.; Pei, Y.; Verdaguer, M.; Renard, J. P.; Sletten, J. *J. Am. Chem. Soc.* **1988**, *110*, 782.
(12) Caneschi, A.; Gatteschi, D.; Renard, J. P.; Rey, P.; Sessoli, R. *Inorg. Chem.*, in press.
(13) Lloret, F.; Nakatani, K.; Journaux, Y.; Kahn, O.; Pei, Y.; Renard, J. P.; *J. Chem. Soc., Chem. Commun.* **1988**, 642.

0002-7863/89/1511-5739$01.50/0 © 1989 American Chemical Society

$MnCu(obbz)\cdot 1H_2O$ is one of the compounds synthesized in the frame of our program concerning the molecular magnetic materials. Our specific strategy to design molecular-based compounds exhibiting a spontaneous magnetization consists of assembling ordered bimetallic chains within the crystal lattice in a ferromagnetic fashion.[14] If, as is most often the case, the intrachain interactions between nearest-neighbor metal ions A and B are antiferromagnetic, the chains are said to be ferrimagnetic and their ground state may be schematized as

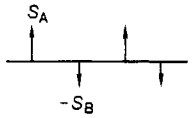

where S_A and S_B ($S_A \neq S_B$) are the local spins. In the absence of any interchain interaction, the magnetic properties of such a system are quite characteristic. The $\chi_M T$ versus T plot, χ_M being the molar magnetic susceptibility per AB unit and T the temperature, exhibits a minimum. Upon cooling below the temperature of this minimum, $\chi_M T$ increases in a ferromagnetic-like fashion and diverges when T approaches zero.[15] This divergence may be considered as the onset of a magnetic ordering at 0 K. It is indeed well established that there is no magnetic ordering at a finite temperature for a purely one-dimensional system.[16] In fact, the chains cannot be perfectly isolated within the lattice. Either they interact between them in an antiferromagnetic fashion and the divergence of $\chi_M T$ is stopped at a certain temperature close to the temperature of three-dimensional ordering[17,18] or they interact in a ferromagnetic fashion, and below a critical temperature, the system behaves as a ferromagnet.[11] Our goal is to realize the conditions leading to this latter situation.

The main requirements of our strategy are the following: (i) $|S_A - S_B|$ must be as large as possible. For that, we utilize Mn(II) and Cu(II) magnetic centers with $^5/_2$ and $^1/_2$ local spins, respectively. (ii) The intrachain antiferromagnetic interactions must be as large as possible. This condition is satisfied when using bridging groups known for their ability to transmit the electronic effects, like the conjugated bisbidentate ligands.[19] (iii) Finally, the relative positions of the chains within the crystal lattice must favor the ferromagnetic situation instead of the antiferromagnetic one. In spite of the successes already obtained, this third requirement is still difficult to control properly.

The first two requirements led us to synthesize bimetallic chain compounds according to one of the two schemes shown below, with Mn(II) cations reacting on copper(II) mononuclear anionic bricks:

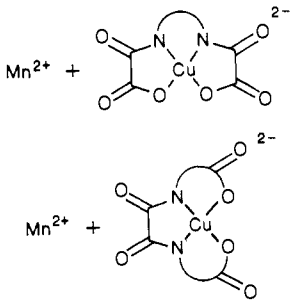

The former scheme gives equally spaced bimetallic chains[11,17] and the latter alternating bimetallic chains.[20] In this paper, we work according to this latter scheme with the brick $[Cu(obbz)]^{2-}$.

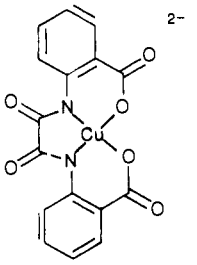

The paper is organized as follows: We first describe the synthesis of the three compounds $MnCu(obbz)\cdot 5H_2O$, $MnCu(obbz)\cdot 1H_2O$, and $NiCu(obbz)\cdot 6H_2O$, hereafter abbreviated as $MnCu\cdot 5H_2O$, $MnCu\cdot 1H_2O$, and NiCu, respectively. Only the third compound has been obtained in the form of single crystals suitable for X-ray work. Although it is isomorphous with none of the MnCu compounds, we describe its structure, which provides information on the copper(II) coordination sphere. We then discuss the powder X-ray patterns, and the XANES and EXAFS spectra of $MnCu\cdot 5H_2O$ and $MnCu\cdot 1H_2O$. X-ray absorption spectroscopy is more and more widely used, with the availability of intense synchrotron radiation. It gives radial distribution function from Extended X-ray Absorption Fine Structure (EXAFS), while exploration of near-edge structure, X-ray Absorption Near-Edge Structure (XANES) gives insights into the electronic structure and the stereochemistry of the absorber. EXAFS cannot provide detailed bond distances and angles far from the absorbing center, as does X-ray diffraction, but its strength lies in the fact that it can lead to an accurate description of the surroundings of the absorbing center without need of long-range order in the material, hence no single crystal. The heart of this paper is devoted to the magnetic properties of the compounds. We show, in particular, that $MnCu\cdot 1H_2O$ orders ferromagnetically at 14 K. The EPR spectra of $MnCu\cdot 5H_2O$ and $MnCu\cdot 1H_2O$ are compared. Finally, we discuss our results in the perspective of the design of novel molecular-based ferromagnets.

Experimental Section

Syntheses. They were carried out in three steps for $MnCu\cdot 5H_2O$ and NiCu, and four steps for $MnCu\cdot 1H_2O$. The first one concerned the synthesis of oxamide bis(2-benzoic) acid (H_4obbz). This ligand was obtained by adding dropwise 1.3 g (10^{-2} mol) of oxalyl chloride to a solution of 3.0 g (2.2×10^{-2} mol) of anthranilic acid in 50 mL of THF. H_4obbz precipitated as a white solid and was filtered, washed with THF, and dried. The yield was 86%. The second step consisted of synthesizing the mononuclear complex $Na_2[Cu(obbz)]\cdot 4H_2O$. For that, 1.3 g ($4 \times 10^{-3}$ mol) of H_4obbz were dissolved in 250 cm^3 of an aqueous solution containing 0.8 g (20×10^{-3} mol) of NaOH; 25 mL of an aqueous solution containing 0.96 g (4×10^{-3} mol) of $Cu(NO_3)_2\cdot 3H_2O$ was then added slowly under stirring. The deep blue-green solution was filtered and then allowed to evaporate slowly. $Na_2[Cu(obbz)]\cdot 4H_2O$ was obtained as a purple polycrystalline powder and filtered. The yield was 56%. Anal. Calcd for $C_{16}H_{20}N_2O_{10}Na_2Cu$: C, 37.98; H, 3.17; N, 5.54; Na, 9.03. Found: C, 38.03; H, 3.10; N, 5.42; Na, 8.99. $MnCu(obbz)\cdot 5H_2O$ was obtained as follows: A 0.22-g aliquot (0.5×10^{-3} mol) of $Na_2[Cu(obbz)]\cdot 4H_2O$ was dissolved in 200 mL of water. The blue solution was then filtered, and 20 mL of an aqueous solution containing 0.18 g (0.5×10^{-3} mol) of $Mn(ClO_4)_2\cdot 6H_2O$ was added slowly, affording a pale green precipitate that was filtered, washed with water, and dried in a desiccator containing silica gel. Anal. Calcd for $C_{16}H_{22}N_2O_{11}CuMn$: C, 36.06; H, 3.38; N, 5.26; Cu, 11.93; Mn, 10.31. Found: C, 35.61; H, 2.99; N, 5.12; Cu, 11.64; Mn 10.13. NiCu was prepared in the same way as $MnCu\cdot 5H_2O$, by replacing manganese(II) perchlorate by nickel(II) perchlorate. Anal. Calcd for $C_{16}H_{24}N_2O_{12}CuNi$: C, 34.64; H, 3.61; N, 5.05; Cu, 11.46; Ni, 10.59. Found: C, 34.67; H, 3.46; N, 4.82; Cu 11.52; Ni, 10.30. Single crystals of NiCu were obtained by slow diffusion of the aqueous solutions of the reactants in an H-shaped tube. Finally, $MnCu\cdot 1H_2O$ was easily prepared by dehydration of $MnCu\cdot 5H_2O$ under vacuum at room temperature or by heating around 65 °C under ambient pressure. The departure of four water molecules was confirmed by thermogravimetric analysis. Anal. Calcd for $C_{16}H_{14}N_2O_7CuMn$: C, 41.70; H, 2.17; N, 6.08; Cu, 13.79; Mn, 11.92. Found: C, 41.91; H, 1.91; N, 6.44, Cu; 13.34; Mn 12.49.

Crystallographic Data Collection and Structure Determination. Information concerning conditions for crystallographic data collection and structure refinement is summarized in Table I. The crystals are red-

(14) Journaux, Y.; Van Koningsbruggen, P.; Lloret, F.; Nakatani, K.; Pei, Y.; Kahn, O.; Renard, J. P. *J. Phys. (Paris)* **1988**, *49*, C8-851.
(15) Verdaguer, M.; Julve, M.; Michalowicz, A.; Kahn, O. *Inorg. Chem.* **1983**, *22*, 2624.
(16) Carlin, R. L. *Magnetochemistry*; Springer-Verlag: Berlin, 1986.
(17) Pei, Y.; Verdaguer, M.; Kahn, O.; Sletten, J.; Renard, J. P. *Inorg. Chem.* **1987**, *26*, 138.
(18) Gleizes, A.; Verdaguer, M. *J. Am. Chem. Soc.* **1984**, *106*, 3727.
(19) Kahn, O. *Angew. Chem., Int. Ed. Engl.* **1985**, *24*, 834.
(20) Pei, Y.; Kahn, O.; Sletten, J.; Renard, J. P.; Georges, R.; Gianduzzo, J.-C. Curely, J.; Xu, Q. *Inorg. Chem.* **1988**, *27*, 47.

Table I. Information Concerning the Crystallographic Data Collection and Refinement Conditions for $[NiCu(obbz)(H_2O)_4]\cdot 2H_2O$

mol formula	$CuNiO_{12}N_2C_{16}H_{20}$
formula wt	554.59
space group	$P2_1/n$ (No. 14)
temp at cryst, K	293
unit cell	
a, Å	7.764 (1)
b, Å	12.559 (3)
c, Å	20.083 (3)
β, deg	97.56 (2)
V, Å^3	1941 (1)
Z	4
D_{expt}, g cm^{-3}	1.898
μ(Mo Kα), cm^{-1}	21.42
range of transm factors	0.75–0.91
cryst size, mm	0.14 × 0.43 × 0.45
instrument	CAD-4
scan type	ω
scan range, $\Delta\omega$, deg	0.7 + 0.35 tan θ
scan speed, deg/min	2
radiation (λ, Å)	monochromated Mo Kα (0.71073)
max 2θ, deg	50
no. reflcns measd	3409
no. reflcns obsd, NO	2539
limit of obsd reflcns	$F_o > 2\sigma$
no. variables refined, NV	362
extinctn coeff	9.08×10^{-8}
agreement factors[a]	
R	0.040
R_w	0.038
s	1.58

[a] Agreement factors are defined as follows: $R = \sum||F_o| - |F_c||\sum|F_o|$: $R_w = [\sum w(|F_o| - |F_c|)^2/\sum w|F_o|^2]^{1/2}$; $s = [\sum w(|F_o| - |F_c|)^2/(NO - NV)]^{1/2}$. The weighting scheme is defined by $w = 1/\sigma_F^2$; $\sigma_F = \sigma_I/(ILp)^{1/2}$; $\sigma_I = [\sigma_c^2 + (0.02N_{net})^2]^{1/2}$. Atomic scattering factors and programs used are those of ref 39 and 40.

dish-brown platelets, limited by faces (0,1,0), (0,−1,0), (0,0,1), (0,0,−1), (1,0,−1), and (−1,0,1). Cell dimensions were determined from 22 reflections with 2θ angles between 13 and 20°. Three reference reflections were monitored throughout the data collection and showed no sign of deterioration.

The structure was solved by direct methods. Cu, Ni, the coordinated atoms, and the two oxamido carbon atoms were revealed in the E map, the remaining non-hydrogen atoms were located in two subsequent Fourier maps. After anisotropic refinement, hydrogen atoms were located in a difference Fourier map and were refined with isotropic thermal parameters. Hydrogen atoms on water O12 could not be unambiguously located, the two highest peaks in the O12 vicinity were chosen, and hydrogen atoms H121 and H122 were kept fixed in the final refinement. The refinement converged at $R = 0.040$, $R_w = 0.038$, $s = 1.58$. Atomic parameters for non-hydrogen atoms are listed in Table II. Anisotropic thermal parameters of non-hydrogen atoms are listed in Table SVII, and coordinates of hydrogen atoms in Table SVIII (Supplementary Material).

EXAFS and XANES Measurements. The spectra were recorded at LURE, the French synchrotron radiation facility, with the EXAFS III spectrometer. This station is equipped with a two-crystal Si 311 monochromator. We used air-filled ionization chambers to measure the flux intensity at the copper edge, before and after the sample, and a helium–neon mixture in the first chamber at the manganese edge. During the experiment, the storage ring used 1.85 GeV positrons with an average intensity of ~150 mA. Harmonics rejection was ensured by slightly detuning the monochromator. The XANES spectra were recorded step by step, every 0.25 eV with 1-s accumulation time per point. The spectrum of a 8-μm-thick metallic foil was recorded just after or just before an unknown XANES spectrum to check energy calibration. This ensures an energy accuracy determination of 0.25 eV. The EXAFS spectra were recorded in the same way within a 1000-eV energy range, with 2-eV steps and 1-s accumulation time per point. The entrance slit was 0.5 mm in both cases. The samples were conditioned as finely ground powders, uniformly dispersed between two X-ray transparent adhesive tapes. The thickness was computed to avoid saturation effects. The absorbance jump at the edge was typically one.

Processing of XANES and EXAFS Data. All the XANES spectra were treated by subtracting from the experimental spectrum a linear background, determined by least-squares fitting to the preedge experimental points; the experiment was calibrated by using as energy reference the maximum of the well-defined peak in the edge of the metallic foil spectrum of copper; the value retained for this point was 8991.1 eV. We verified that the first inflection point in the spectrum of the manganese foil was 6539 eV. The spectra were normalized by taking the EXAFS background extrapolation as unit absorbance. The energy of the preedge transition was determined by fitting the experimental curves with polynomial functions and by taking the first and the second derivatives. Data processing used home-written programs running on microcomputers.

The EXAFS analysis followed the classical way, already described.[21,22] We subtracted the background by a linear function, fitted from the experimental points before the edge and the atomic absorption μ_o by fitting with a polynomial function, to obtain the $k^*\chi(k)$ EXAFS signal in the k space. Then, we got a Fourier transform of the EXAFS signal in the distance R space using a k^3 ponderation (k is the wave vector associated with the ejected photoelectron). We used the experimental data between $k_{min} = 3$ Å^{-1} and $k_{max} = 11$ Å^{-1}. We then filtered the region of interest in the Fourier transform, using a Hamming window, and we performed an inverse Fourier transform back to k space. We analyzed the first shell by a one-shell least-squares fitting procedure with the help of the MINUIT program from the CERN library, and Teo and Lee tabulated amplitude and phase shifts.[21,23] As usual, $E°$ was included as a fitting parameter for the fitted shells. The mean free path of the photoelectron was considered as linear in k, the proportionality constant being a fitting parameter. The number of neighbors was fixed, and a scaling factor was then introduced as a fitting parameter.[24]

Magnetic Measurements. In the 4.2–300 K temperature range, these were carried out with a Faraday-type magnetometer equipped with a helium continuous-flow cryostat. $HgCo(NCS)_4$ was used as a susceptibility standard. Diamagnetic corrections were taken as −335 cm^3 mol^{-1} for NiCu, -325×10^{-6} cm^3 mol^{-1} for $MnCu\cdot 5H_2O$ and -275×10^{-6} cm^3

Table II. Atomic Parameters for Non-Hydrogen Atoms for $[NiCu(obbz)(H_2O)_4]\cdot 2H_2O$[a]

atom	x	y	z	B_{eq}, Å^2
Cu	0.50883 (7)	0.74037 (4)	0.53696 (2)	2.01 (1)
Ni	0.24923 (7)	0.73446 (5)	0.28287 (3)	2.28 (1)
O1	0.4390 (4)	0.8068 (2)	0.3444 (1)	2.78 (7)
O2	0.2402 (4)	0.6484 (3)	0.3680 (1)	3.01 (7)
O3	0.6298 (4)	0.8415 (2)	0.5966 (I)	2.67 (7)
O4	0.4891 (4)	0.6600 (2)	0.6159 (1)	2.92 (7)
O5	0.7940 (4)	0.9741 (3)	0.6329 (2)	3.24 (7)
O6	0.4039 (5)	0.5414 (3)	0.6832 (2)	3.41 (8)
O7	0.4174 (4)	0.6239 (3)	0.2496 (2)	3.31 (8)
O8	0.0691 (5)	0.8482 (3)	0.3042 (2)	4.61 (9)
O9	0.0426 (4)	0.6602 (2)	0.2263 (1)	2.60 (7)
O10	0.2970 (5)	0.8210 (3)	0.2023 (2)	4.27 (8)
O11	0.5522 (5)	0.9634 (3)	0.2196 (2)	4.29 (9)
O12	0.7290 (6)	0.7416 (3)	0.2438 (3)	6.3 (1)
N1	0.5439 (4)	0.8198 (3)	0.4577 (2)	1.64 (7)
N2	0.3626 (4)	0.6438 (3)	0.4800 (2)	1.77 (7)
C1	0.4505 (5)	0.7785 (3)	0.4047 (2)	1.92 (8)
C2	0.3394 (5)	0.6810 (3)	0.4182 (2)	1.97 (9)
C3	0.6481 (5)	0.9123 (3)	0.4552 (2)	1.77 (8)
C4	0.7225 (5)	0.9631 (3)	0.5149 (2)	1.75 (8)
C5	0.7136 (6)	0.9246 (3)	0.5854 (2)	2.14 (9)
C6	0.8138 (6)	1.0576 (3)	0.5097 (2)	2.5 (1)
C7	0.8400 (6)	1.1012 (4)	0.4496 (2)	2.8 (1)
C8	0.7763 (6)	1.0479 (4)	0.3916 (2)	3.0 (1)
C9	0.6831 (6)	0.9554 (4)	0.3946 (2)	2.8 (1)
C10	0.2889 (5)	0.5470 (3)	0.4998 (2)	1.81 (9)
C11	0.3082 (6)	0.5159 (3)	0.5672 (2)	1.93 (9)
C12	0.4052 (6)	0.5757 (3)	0.6250 (2)	2.25 (9)
C13	0.2354 (6)	0.4190 (4)	0.5843 (2)	2.5 (1)
C14	0.1455 (6)	0.3541 (3)	0.5373 (2)	2.6 (1)
C15	0.1294 (6)	0.3837 (4)	0.4708 (2)	2.8 (1)
C16	0.1999 (6)	0.4785 (4)	0.4524 (2)	2.5 (1)

[a] The isotropic equivalent thermal parameter is given as $B_{eq} = {}^4/_3\sum_i\sum_j\beta_{ij}a_ia_j$.

(21) Teo, B. K. *EXAFS, Basic Principles and Data Analysis*; Springer Verlag: Berlin, 1986.
(22) Michalowicz, A.; Verdaguer, M.; Mathey, Y.; Clement, R. *Top. Curr. Chem.* **1988**, *145*, 107.
(23) Teo, B. K.; Lee, P. A. *J. Am. Chem. Soc.* **1979**, *101*, 2815.
(24) The programs are written in FORTRAN 77 and are freely available from the Computing Center of The Université de Paris-Sud. An up-to-date version for Macintosh microcomputer is also available.

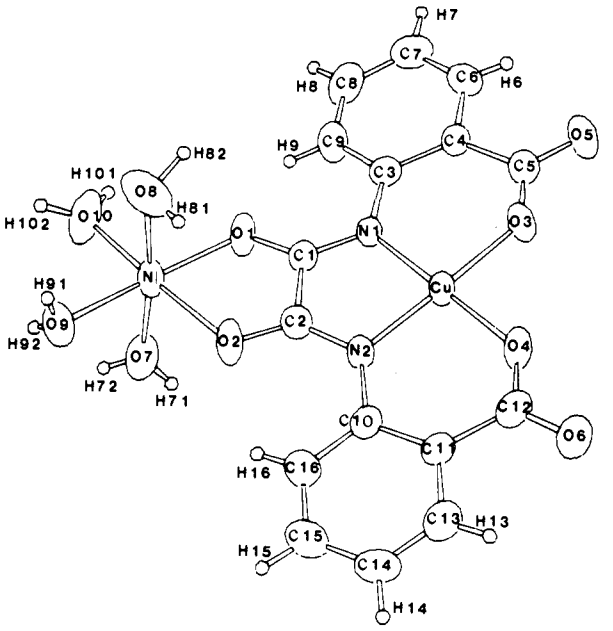

Figure 1. Perspective view of $NiCu(obbz)(H_2O)_4$. Thermal ellipsoids of non-hydrogen atoms are plotted at the 70% probability level. Hydrogen atoms are given an arbitrary radius.

Table III. Bond Distances (Å) Involving Non-Hydrogen Atoms for $[NiCu(obbz)(H_2O)_4]\cdot 2H_2O$

atom 1	atom 2	distance	atom 1	atom 2	distance
Cu	O3	1.906 (2)	N1	C3	1.420 (4)
Cu	O4	1.903 (2)	N2	C2	1.316 (5)
Cu	N1	1.928 (3)	N2	C10	1.422 (4)
Cu	N2	1.930 (3)	C1	C2	1.542 (5)
Ni	O1	2.011 (2)	C3	C4	1.413 (4)
Ni	O2	2.031 (2)	C3	C9	1.391 (5)
Ni	O7	2.076 (3)	C4	C5	1.505 (5)
Ni	O8	2.083 (4)	C4	C6	1.394 (5)
Ni	O9	2.062 (3)	C6	C7	1.365 (5)
Ni	O10	2.024 (4)	C7	C8	1.377 (5)
O1	C1	1.254 (4)	C8	C9	1.375 (5)
O2	C2	1.254 (4)	C10	C11	1.399 (4)
O3	C5	1.266 (4)	C10	C16	1.396 (5)
O4	C12	1.269 (4)	C11	C12	1.500 (5)
O5	C5	1.237 (5)	C11	C13	1.404 (6)
O6	C12	1.246 (5)	C13	C14	1.368 (5)
N1	C1	1.313 (4)	C14	C15	1.375 (5)
			C15	C16	1.381 (5)

mol^{-1} for $MnCu\cdot 1H_2O$. Magnetic measurements below 4.2 K were performed with a mutual inductance bridge working in zero field. Magnetization measurements in the 0–50-G field range were carried out with a laboratory-made low-field SQUID magnetometer, and magnetization data above 50 G were recorded with a laboratory-made apparatus working according to the extraction method.

EPR Spectra. The X-band powder EPR spectra were recorded at various temperatures between 4.2 and 300 K with a ER 200D Bruker spectrometer equipped with a helium continuous-flow cryostat, a Hall probe, and a frequency meter.

Structural Investigations

NiCu. The structure of $NiCu(obbz)(H_2O)_4\cdot 2H_2O$ consists of neutral heterodinuclear units as shown in Figure 1 and noncoordinated water molecules. Bond lengths and angles involving non-hydrogen atoms are listed in Tables III and IV. The Ni atom has somewhat distorted octahedral surroundings with two oxygen atoms of the oxamido group and four water molecules in the coordination sphere. The Cu environment may be described as square planar with a slight tetrahedral distortion, the axial positions being screened by carbon atoms in neighboring molecules related by inversion centers with Cu···C7 $(1-x, 2-y, 1-z) = 3.400$ Å and C···C15 $(1-x, 1-y, 1-z) = 3.234$ Å. The dihedral angle through the best equatorial least-squares planes of Ni (O1, O2, O9, O10) and Cu (O3, O4, N1, N3) is 17.0°. The Cu···Ni distance within the binuclear unit is 5.235 (1) Å.

Table IV. Bond Angles (deg) Involving Non-Hydrogen Atoms for $[NiCu(obbz)(H_2O)_4]\cdot 2H_2O$

atom 1	atom 2	atom 3	angle
O3	Cu	O4	85.2 (2)
O3	Cu	N1	93.7 (2)
O3	Cu	N2	173.6 (1)
O4	Cu	N1	176.5 (1)
O4	Cu	N2	93.2 (1)
N1	Cu	N2	88.3 (1)
O1	Ni	O2	80.03 (9)
O1	Ni	O7	93.5 (1)
O1	Ni	O8	91.3 (1)
O1	Ni	O9	175.2 (1)
O1	Ni	O10	93.0 (1)
O2	Ni	O7	90.4 (1)
O2	Ni	O8	95.3 (1)
O2	Ni	O9	96.5 (1)
O2	Ni	O10	171.4 (1)
O7	Ni	O8	173.1 (1)
O7	Ni	O9	89.8 (1)
O7	Ni	O10	85.0 (1)
O8	Ni	O9	85.9 (1)
O8	Ni	O10	89.7 (2)
O9	Ni	O10	90.8 (1)
Ni	O1	C1	114.7 (2)
Ni	O2	C2	114.7 (2)
Cu	O3	C5	131.4 (2)
Cu	O4	C12	131.5 (2)
Cu	N1	C1	110.1 (2)
Cu	N1	C3	126.5 (2)
C1	N1	C3	123.5 (3)
Cu	N2	C2	109.5 (2)
Cu	N2	C10	126.7 (2)
C2	N2	C10	123.8 (3)
O1	C1	N1	129.3 (3)
O1	C1	C2	115.2 (3)
N1	C1	C2	115.7 (3)
O2	C2	N2	129.5 (3)
O2	C2	C1	114.7 (3)
N2	C2	C1	115.9 (3)
N1	C3	C4	120.8 (4)
N1	C3	C9	121.8 (3)
C4	C3	C9	117.5 (3)
C3	C4	C5	126.1 (4)
C3	C4	C6	118.4 (3)
C5	C4	C6	115.6 (3)
O3	C5	O5	119.7 (3)
O3	C5	C4	121.4 (4)
O5	C5	C4	118.9 (3)
C4	C6	C7	123.1 (4)
C6	C7	C8	118.4 (4)
C7	C8	C9	120.3 (4)
C3	C9	C8	122.3 (4)
N2	C10	C11	120.9 (4)
N2	C10	C16	121.2 (3)
C11	C10	C16	117.9 (3)
C10	C11	C12	126.1 (3)
C10	C11	C13	119.0 (3)
C12	C11	C13	115.0 (3)
O4	C12	O6	119.4 (3)
O4	C12	C11	121.4 (3)
O6	C12	C11	119.2 (3)
C11	C13	C14	122.2 (4)
C13	C14	C15	118.8 (4)
C14	C15	C16	120.3 (4)
C10	C16	C15	121.8 (4)

The packing of the molecules in the crystal lattice is illustrated in Figure 2. The shortest intermolecular distance between metal atoms is Cu···Ni $(^1/_2 + x, ^3/_2 - y, ^1/_2 + z) = 5.054$ (1) Å. Cu and Ni then belong to molecules related by the *n* glide. Furthermore, across inversion centers, there are Cu···Cu $(1-x, 1-y, 1-z)$ distances of 6.215 (1) Å, and between molecules related by screw-axes Ni···Ni $(^1/_2 - x, ^1/_2 + y, ^1/_2 - z)$ distance of 6.417 (1) Å.

The molecules are connected through an extensive network of hydrogen bonds involving oxygen atoms belonging to carboxylato

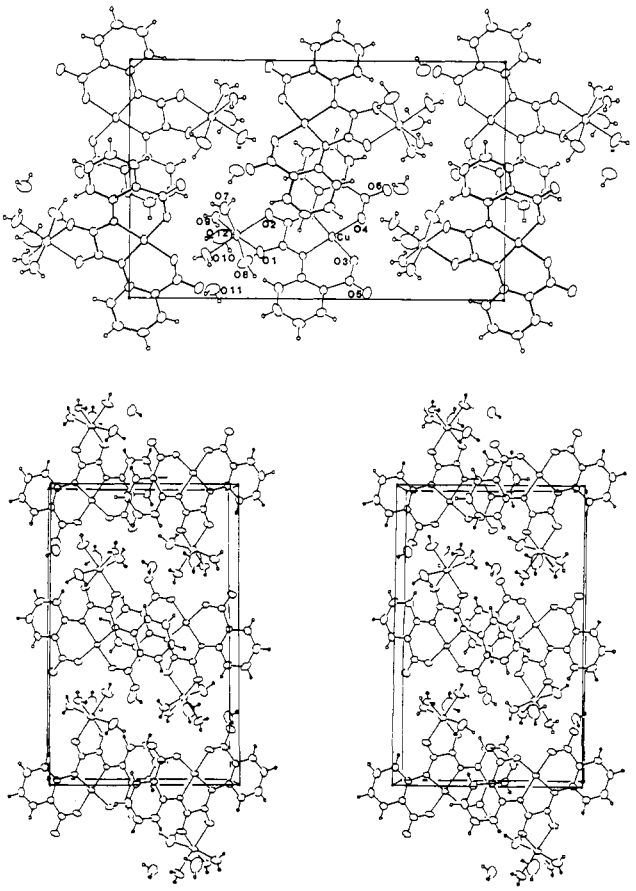

Figure 2. Top: Crystal packing for $NiCu(obbz)(H_2O)_4\cdot 2H_2O$, projected down to the a axis. The origin is in the upper left-hand corner. Bottom: Stereopicture of crystal packing as viewed down the a axis. The origin is the lower left-hand corner, with the b axis running horizontally.

Table V. Compared Spacing (Å) of the Strongest Lines of the X-ray Powder Patterns for $MnCu\cdot 5H_2O$ and $MnCu\cdot 1H_2O$

	$MnCu\cdot 5H_2O$	$MnCu\cdot 1H_2O$
very strong	3.36	3.03
medium	4.50	4.08
weak	3.83	3.58
strong	3.31	3.20
medium	2.34	2.26

groups as well as to coordinated and noncoordinated water molecules. A list of hydrogen bonds is given in Table SIX.

$MnCu\cdot 5H_2O$ and $MnCu\cdot H_2O$. In spite of many attempts, we have not been able yet to grow single crystals of $MnCu\cdot 5H_2O$ or $MnCu\cdot 1H_2O$ and we have decided to use alternative techniques to get structural information for the two compounds. First, we recorded the X-ray powder patterns of both compounds. The two patterns are actually almost identical, as pointed out in Table V. The only difference is a weak shrinkage effect in $MnCu\cdot 1H_2O$, as compared to $MnCu\cdot 5H_2O$. This result strongly suggests that the two structures are basically identical, with four noncoordinated additional water molecules in the $MnCu\cdot 5H_2O$ phase. In other words, in both compounds, only one water molecule would be bonded to a metal atom. This assumption is substantiated by the study of the XANES and EXAFS spectra, as discussed below.

XANES and EXAFS Spectra. We recorded the X-ray absorption spectra at both the copper and manganese edges.

Copper Edge. The XANES spectra of the two compounds at the copper edge are given in Figure 3. Two facts emerge from this figure: (i) The two spectra are almost identical as to their shapes and the transition energies. The loss of four water molecules does not perturb the copper coordination sphere. (ii) The low-energy side of the edge exhibits the shoulder characteristic of copper(II) in elongated tetragonal surroundings.[25-27] The top

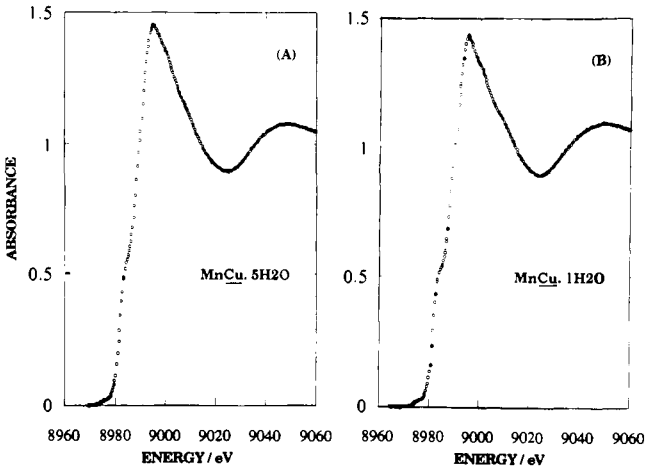

Figure 3. Copper-edge spectra of compounds $MnCu\cdot 5H_2O$ (A) and $MnCu\cdot 1H_2O$ (B).

Table VI. EXAFS Results for the First Coordination Sphere

		N^a	R, Å	σ, Å	Γ^b	S^b	$\rho^{c,d}$ (×10⁻³)
Around Copper							
$MnCu\cdot 5H_2O$	Cu–(O,N)	4	1.93 (2)	0.07	1.2	1.14	4
$MnCu\cdot 1H_2O$	Cu–(O,N)	4	1.95 (2)	0.07	1.2	1.10	3
Around Manganese							
$MnCu\cdot 5H_2O$	Mn–(O)	6	2.17	0.09	1.10	1.07	6
$MnCu\cdot 1H_2O$	Mn–(O)	6	2.16	0.08	1.10	1.11	9

[a] The number of neighbors was fixed. [b] The mean electron-free path λ was chosen as $\lambda = k/\Gamma$; Γ was first allowed to vary, with S fixed and then fixed with S as a fitted variable. [c] ρ is the agreement factor defined as $\rho = \sum\omega_i(\chi^i_{exp} - \chi^i_{theo})^2$ with $\omega_i = 0$ for $k \leq 3$ Å^{-1} and $\omega_i = 1$ for $k \geq 3$ Å^{-1}. [d] The fitted was obtained with ΔE^0 as a fitting parameter. E^0 was the energy of the maximum of the edge. The value of ΔE^0 was the same for both compounds at the copper edge (10 eV) and at the manganese edge (6.5 eV).

of the edge is at 14.3 eV. The energy gap between this shoulder and the preedge is equal to 8.6 eV, which gives an estimate for the destabilization of the $4p_z$ metal orbital, z being the elongation axis. This value is close to that found in $[Cu(en)_2](NO_3)_2$ with en = ethylenediamine, i.e., 8.7 eV.[28] It has been suggested that in elongated tetragonal copper(II) complexes, the more apart from the metal ion the apical site(s), the more displaced toward the low energies this shoulder.[25-27] In the present case, the copper(II) ion appears to be in an essentially square-planar environment. The axial ligands, if any, are very far from the metal.

The EXAFS spectra and their Fourier transforms are shown in Figure 4. Again, the two spectra are very similar. The fit of the first shell gives an average value of the Cu–O and Cu–N distances equal to 1.93 (2) Å for $MnCu\cdot 5H_2O$ and 1.95 (2) Å for $MnCu\cdot 1H_2O$, as shown in Table VI. These values agree with those determined by X-ray crystallography for NiCu where the copper(II) ion has the same square-planar environment (see Table III). Experimental and calculated EXAFS spectra are compared in Figure S13.

Manganese Edge. The XANES spectra of the two compounds at the manganese edge are compared in Figure 5. These spectra are typical of manganese(II) in octahedral surroundings.[29,30] The intensity of the preedge is weak, which indicates that Mn(II) is located on a (quasi) inversion center.[31,32] The top of the edge

(25) Bair, R. A.; Goddard, W. A. *Phys. Rev. B* **1980**, *22*, 2767.
(26) Kosugi, N.; Yokoyama, T.; Asakuna, K.; Kuroda, H. *Chem. Phys.* **1984**, *91*, 249.
(27) Smith, T. A.; Penner-Hahn, J. E.; Berding, M. A.; Doniach, S.; Hodgson, K. O. *J. Am. Chem. Soc.* **1985**, *107*, 5945.
(28) Carriat, J. Y.; Verdaguer, M., unpublished result.
(29) Belli, M.; Scarfati, A.; Bianconi, A.; Mobilio, S.; Palladino, L.; Reale, A.; Burattini, E. *Solid State Commun.* **1980**, *35*, 355.
(30) Cartier, C.; Verdaguer, M.; Menage, S.; Girerd, J. J.; Tuchagues, J. P.; Mabad, B. *J. Phys. (Les Ulis)* **1986**, *47*, C8-623.
(31) Cartier, C. Ph.D. Thesis, Université de Paris-Sud, 1988.

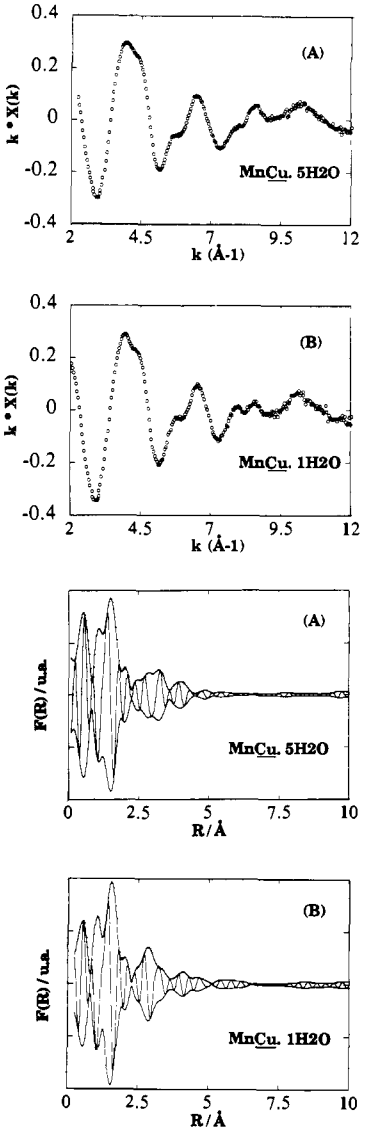

Figure 4. EXAFS spectra (top) $k\chi(k)$ at the copper edge and Fourier transforms (bottom) of $k^3\chi(k)$ for compounds $MnCu{\cdot}5H_2O$ (A) and $MnCu{\cdot}1H_2O$ (B).

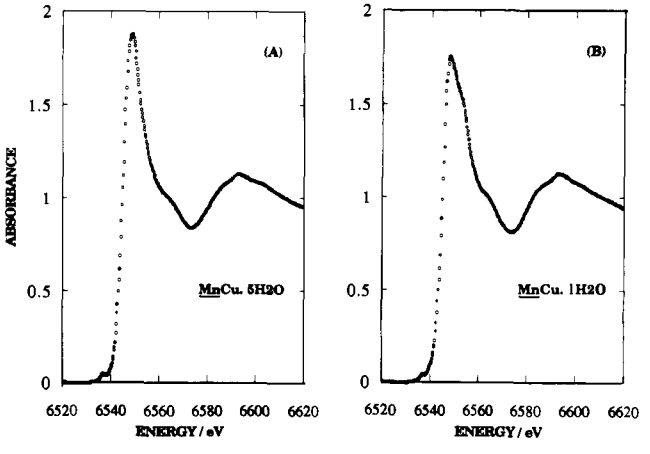

Figure 5. Manganese-edge spectra of compounds $MnCu{\cdot}5H_2O$ (A) and $MnCu{\cdot}1H_2O$ (B).

for $MnCu{\cdot}5H_2O$ is featureless, which shows that the deformation of the octahedral environment, if any, is weak. Two evolutions

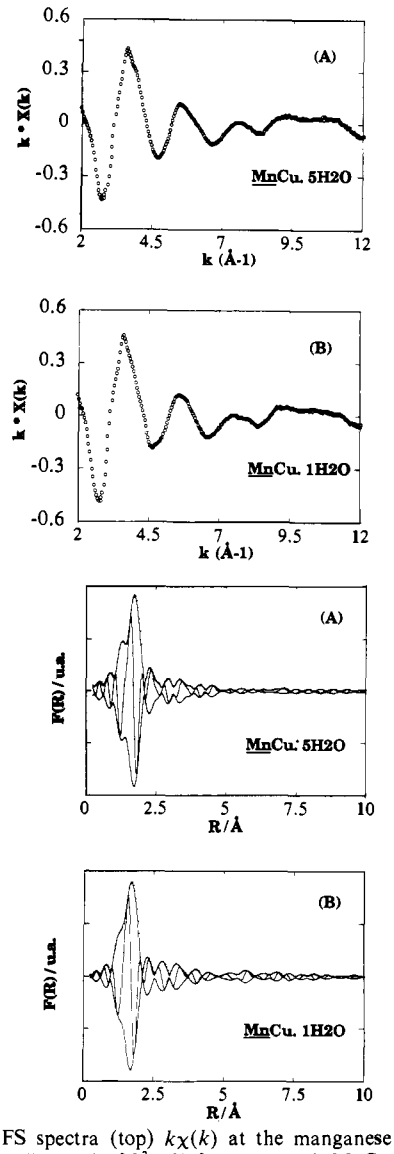

Figure 6. EXAFS spectra (top) $k\chi(k)$ at the manganese edge and Fourier transforms (bottom) of $k^3\chi(k)$ for compounds $MnCu{\cdot}5H_2O$ (A) and $MnCu{\cdot}1H_2O$ (B).

may be noted when passing from $MnCu{\cdot}5H_2O$ to the dehydrated form $MnCu{\cdot}1H_2O$. The main "white line" is less intense and a shoulder is observed in the high-energy side of the edge. This region of the absorption spectrum is the most difficult to interpret. Actually, two interpretations are possible; either transition to bound states, or full or intermediate scattering scheme.[33-36] The observed evolutions would be assigned to a splitting of the t_{1u}* metal orbitals in the frame of the former interpretation, and to slightly different multiple scattering pathways in the frame of the latter. The two views, however, converge to the same conclusion. The decrease of the white line and the appearance of a high-energy shoulder are consistent with a distortion of the octahedral environment in $MnCu{\cdot}1H_2O$.

The EXAFS spectra and their Fourier transforms are compared in Figure 6. The differences between the spectra themselves as well as between their Fourier transforms are negligible. In particular, the amplitudes of the EXAFS oscillations appear unchanged when passing from $MnCu{\cdot}5H_2O$ to $MnCu{\cdot}1H_2O$. This result is particularly important since it proves that manganese(II)

(32) Roe, A. L.; Schneider, D. J.; Mayer, R. J.; Pyrz, J. W.; Widom, J.; Que, L., Jr. *J. Am. Chem. Soc.* **1984**, *106*, 1676.

(33) Natoli, C. R.; Misemer, D. K.; Doniach, S.; Kutzler, F. W. *Phys. Rev. A* **1980**, *22*, 1104.

(34) Kutzler, F. W.; Natoli, C. R.; Misemer, D. K.; Doniach, S.; Hodgson, K. O. *J. Chem. Phys.* **1980**, *73*, 3274.

(35) Natoli, C. R.; Benfatto, M.; Doniach, S. *Phys. Rev. A* **1986**, *34*, 4682.

(36) Benfatto, M.; Natoli, C. R.; Garcia, J.; Bianconi, A.; Marcelli, A.; Fanfoni, M.; Davoli, I. *Phys. Rev. B* **1986**, *34*, 5774.

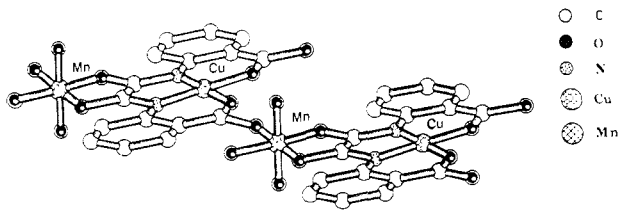

Figure 7. Basic structure proposed for $MnCu\cdot 5H_2O$ and $MnCu\cdot 1H_2O$. The oxygen atoms occupying the apical positions around the Mn(II) ions belong probably to carboxylato groups of adjacent chains.

has the same number of nearest neighbors in both compounds and retains an octahedral environment in the dehydrated-phase $MnCu\cdot 1H_2O$. The fit of the EXAFS data leads to $R = 2.17$ (2) and 2.16 (2) Å for the radius of the first shell around the metal ion in $MnCu\cdot 5H_2O$ and $MnCu\cdot 1H_2O$, respectively (see Table VI). These values are consistent with the average value of the Mn–O distances in the MnCu chain compounds, of which the structure has been solved by X-ray diffraction.[11,17,20] The calculated spectra are compared to the experimental ones in Figure S14.

We would like now to sum up the structural informations arising from the X-ray diffraction powder patterns and the X-ray absorption: (i) $MnCu\cdot 5H_2O$ and $MnCu\cdot 1H_2O$ have very similar structures. The four additional water molecules in the former compound are not coordinated to the metal ions, which explains why they can leave so easily. (ii) Copper(II) is in elongated tetragonal surroundings with apical sites, if any, very apart from the metal. In this respect, it is worth recalling that the Cu–O(apical) distance in $MnCu(obp)(H_2O)_3\cdot H_2O$ with obp = oxamidobis(propionato) is 2.625 (1) Å. (iii) Manganese(II) is in octahedral surroundings for both $MnCu\cdot 5H_2O$ and $MnCu\cdot 1H_2O$. The octahedron seems to be more distorted in the dehydrated form. The average length of the Mn–nearest neighbor bonds is consistent with Mn–O bonds. The problem at hand is then: what are the six atoms surrounding the Mn(II) ion? Clearly, two of them are the oxygen atoms of the oxamido group, one is the oxygen atom of the carboxylato group, and most likely one is the oxygen atom of the water molecule that does not leave under vacuum. The difficulty concerns the nature of the last two nearest neighbors. In the two mononuclear precursors, $[Cu(obbz)]^{2-}$ utilized in this work and $[Cu(obp)]^{2-}$ utilized to synthesize the alternating bimetallic chain $MnCu(obp)(H_2O)_3\cdot H_2O$ previously described,[20] there are two oxygen atoms belonging to carboxylato groups and not bonded equatorially to copper(II). In $MnCu(obp)(H_2O)_3\cdot H_2O$, one of these oxygen atoms is bonded to Mn(II) in trans position with regard to a Mn–O(oxamido) bond. The other one is weakly bonded in an apical position to a Cu(II) belonging to an adjacent chain. In the two MnCu compounds studied in this paper, it is probable that those two oxygen atoms are bonded to a Mn(II) ion. It follows that the compounds $MnCu\cdot 5H_2O$ and $MnCu\cdot 1H_2O$ cannot be structurally described in terms of one-dimensional systems. The description we propose is the following: first we consider the chain shown in Figure 7 with Mn(II) and Cu(II) ions alternately bridged by oxamido and carboxylato groups. The equatorial plane around Mn(II) consists of four oxygen atoms belonging to an oxamido group, a carboxylato group and a water molecule. The apical sites are two other oxygen atoms belonging most probably to carboxylato groups of an adjacent chain, so that we have a two- or three-dimensional packing. Several polymeric structures may then be imagined but in the absence of additional information, it is not possible to rationally choose one of them. Moreover, the existence of Mn–O bonds involving the oxygen atoms of the oxamido group cannot be completely ruled out. In $MnCu\cdot 5H_2O$, we have in addition four noncoordinated water molecules in the crystal lattice.

Magnetic Susceptibilities

The thermal variations of the magnetic susceptibilities are shown in Figure 8 for NiCu and Figure 9 for $MnCu\cdot 5H_2O$ and $MnCu\cdot 1H_2O$, in the form of the $\chi_M T$ versus T plots, χ_M being the molar magnetic susceptibility per NiCu or MnCu unit and T the temperature.

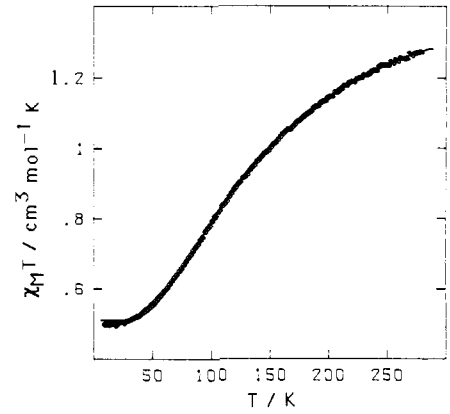

Figure 8. Temperature dependence of $\chi_M T$ for NiCu.

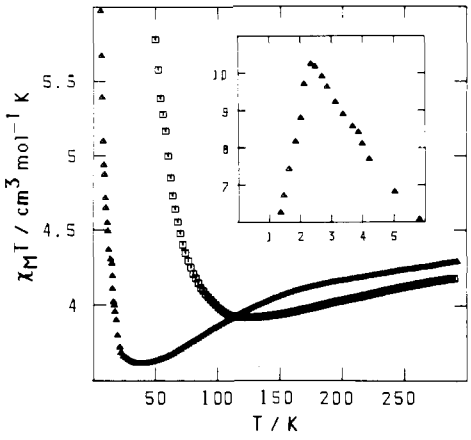

Figure 9. Temperature dependences of $\chi_M T$ for $MnCu\cdot 5H_2O$ (△) and $MnCu\cdot 1H_2O$ (□).

NiCu. The magnetic susceptibility has been studied in the 15–300 K temperature range. $\chi_M T$ is equal to 1.28 cm^3 mol^{-1} K at 290 K, decreases upon cooling, and finally reaches a plateau below 50 K with $\chi_M T = 0.50$ cm^3 mol^{-1} K. This behavior is typical of an isolated Ni(II)Cu(II) pair with antiferromagnetic intramolecular interaction.[2,37] The plateau below 50 K corresponds to the temperature range where only the doublet ground state is thermally populated. The Cu(II)–Ni(II) intermolecular interaction between ions separated by 5.054 (4) Å (see the description of the structure) appears negligible. Otherwise, $\chi_M T$ would increase upon cooling down in the very low temperature range as it does for a bimetallic chain. The magnetic data allow a rather accurate determination of the doublet–quartet energy gap $3J/2$ arising from the intramolecular interaction. The theoretical expression for $\chi_M T$ is[2]

$$\chi_M T = (N\beta^2/4k) \times \left[g_{1/2}^2 + 10g_{3/2}^2 \exp(3J/2kT)\right] \Big/ \left[1 + 2\exp(3J/2kT)\right]$$

where the symbols have their usual meaning.[2,33] The least-squares fitting of the data leads to $3J/2 = -156$ (3) cm^{-1}, $g_{1/2} = 2.32$, and $g_{3/2} = 2.13$.

$MnCu\cdot 5H_2O$. The magnetic susceptibility has been studied in the 1.2–300 K temperature range. $\chi_M T$ is equal to 4.30 cm^3 mol^{-1} K at 290 K, which is close to what is expected for Mn(II) and Cu(II) ions in the high-temperature limit. Upon cooling, $\chi_M T$ decreases and reaches a minimum around 40 K with $\chi_M T = 3.61$ cm^3 mol^{-1} K. Below 40 K, $\chi_M T$ increases again upon cooling further up to a sharp maximum at 2.3 K with $\chi_M T = 10.3$ cm^3 mol^{-1} K and then falls down. This behavior is quantitatively almost identical with that reported for $MnCu(obp)(H_2O)_3\cdot H_2O$. So, in

(37) Journaux, Y.; Kahn, O.; Morgenstern-Badarau, I.; Galy, J.; Jaud, J.; Bencini, A.; Gattesch, D. *J. Am. Chem. Soc.* **1985**, *107*, 6305.

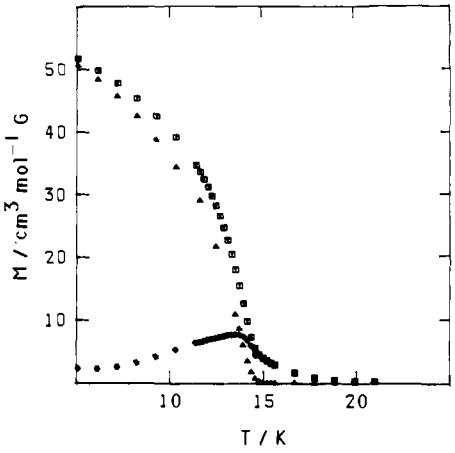

Figure 10. Temperature dependence of the magnetization M for MnCu·1H_2O in the 5–20 K range and with a field of 0.1 G. (□) Field cooled magnetization; (△) remnant magnetization; (◇) zero field cooled magnetization (see text).

spite of its two- or three-dimensional structure, MnCu·5H_2O behaves magnetically as a bimetallic chain with Mn(II) and Cu(II) ions bridged by oxamido and carboxylato groups, respectively, and very weak interchain interactions. This apparent paradox will be discussed in the last section. The magnetic data down to 10 K may be interpreted with the classical–quantum model previously described.[20] The spin Hamiltonian taking into account the Zeeman perturbation to consider is

$$\mathcal{H} = -J\sum_i S_{Cu,i}[(1+\alpha)S_{Mn,i} + (1-\alpha)S_{Mn,i+1}] + \sum_i (g_{Cu}S_{Cu,i} + g_{Mn}S_{Mn,i})\beta H$$

i runs over the MnCu units. $S_{Mn,i}$ and $S_{Cu,i}$ are local spin operators; the former are treated classically and the latter as quantum spins. H is the applied magnetic field. Each Cu(II) ion interacts with two nearest-neighbor Mn(II) ions, the interaction parameters being $J(1+\alpha)$ and $J(1-\alpha)$, respectively. g_{Mn} and g_{Cu} are the local g factors, assumed to be isotropic. The equations leading to the theoretical expression of χ_M are recalled in the Appendix. The least-squares fitting of the experimental data leads to $J = -17$ (2) cm^{-1}, $\alpha = 0.7$ (1), $g_{Mn} = 1.98$ (1), and $g_{Cu} = 2.12$ (3). The uncertainties, relatively large, are estimated by investigating the effect of small changes in the values of the parameters. The two exchange parameters between Mn(II) and Cu(II) nearest-neighbor ions are therefore $J_1 = -29$ (3) cm^{-1} and $J_2 = -5$ (2) cm^{-1}. The J_1 parameter is clearly associated with the exchange pathway involving the oxamido bridge and the J_2 parameter with that involving the carboxylato bridge.[20]

The sharp maximum of $\chi_M T$ occurring at 2.3 K is due to a three-dimensional antiferromagnetic ordering. The same long-range ordering had been observed in MnCu(obp)$(H_2O)_3$·H_2O.

MnCu·1H_2O. Even though, structurally, MnCu·5H_2O and MnCu·1H_2O are very similar, their magnetic properties are quite different. $\chi_M T$ for MnCu·1H_2O is equal to 4.18 cm^3 mol^{-1} K at 290 K, slightly decreases upon cooling down, and reaches a very rounded minimum around 120 K with $\chi_M T = 3.92$ cm^3 mol^{-1} K. Below 120 K, $\chi_M T$ increases more and more rapidly, reaches extremely high values like 50 cm^3 mol^{-1} K at 20 K and 80 cm^3 mol^{-1} K at 17.4 K, and finally diverges. Actually, when approaching 14 K, $\chi_M T$ becomes more and more field dependent, which strongly suggests that a ferromagnetic transition takes place.

For MnCu·5H_2O, the 3-D antiferromagnetic ordering influences the magnetic properties only in the very low temperature range. Otherwise, the $\chi_M T$ versus T plot is characteristic of an antiferromagnetically coupled bimetallic chain, also called ferrimagnetic chain, with the expected minimum of $\chi_M T$. In contrast, for MnCu·1H_2O, the magnetic properties are largely governed by the 3-D ferromagnetic ordering. Only the decrease of $\chi_M T$ in the 300–120 K temperature range is reminiscent of the behavior expected for a bimetallic chain. The minimum of $\chi_M T$ around 120 K is attributed to two- or three-dimensional rather than to one-dimensional effects. Indeed, the $\chi_M T$ versus T plot cannot be fitted properly with the quantum–classical model used for MnCu·5H_2O. In particular, the experimentally observed $\chi_M T$ values below 60 K are much higher than those deduced from the 1-D theoretical model when taking J and α values consistent with the minimum of $\chi_M T$ around 120 K.

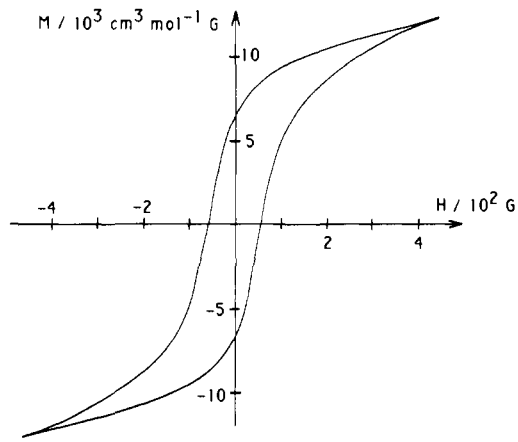

Figure 11. Hysteresis loop $M = f(H)$ for a polycristalline sample of MnCu·1H_2O at 4.2 K.

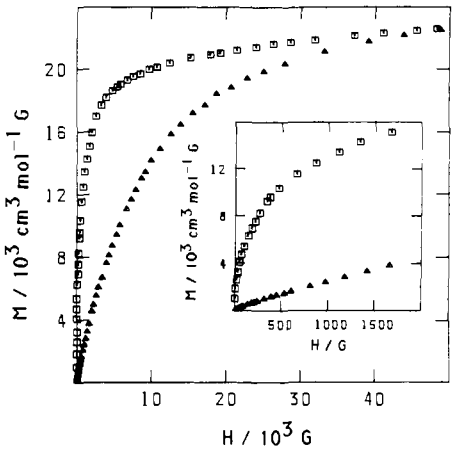

Figure 12. Field dependences of the magnetization M for polycristalline samples of MnCu·5H_2O (△) and MnCu·1H_2O (□).

Magnetization

To confirm the ferromagnetic transition in MnCu·1H_2O, we investigated the variation of the molar magnetization M versus T in a field of 0.1 G, with a SQUID magnetometer. The results are represented in Figure 10. We first measured the field-cooled magnetization (FCM) obtained by cooling down in the field. The curve shows the typical features of a ferromagnetic transition, i.e., a rapid increase of M when T decreases below 15 K and then a break in the curve around $T_c = 14$ K. We then measured the remnant magnetization by switching off the field at 5 K and warming up. The remnant magnetization, as expected, vanishes at T_c. Finally, we measured the zero-field cooled magnetization (ZFCM) by cooling down in zero field and then warming up within the field. At any temperature below T_c, the ZFCM is smaller than the FCM, due to the fact that in this low-temperature range the applied field is too weak to move the domain walls. The ZFCM exhibits a maximum around T_c, as expected for a polycrystalline ferromagnet.[38]

(38) See, for instance: Hitzfeld, M.; Ziemann, P.; Buckel, W.; Claus, H. *Phys. Rev. B* **1984**, *29*, 5023.

(39) Cromer, D. T.; Waber, J. T. *International Tables for X-ray Crystallography*; Kynoch Press: Birmingham, England, 1974; Vol. IV, p 99, Table 2.2B.

(40) Frez, B. A. *The SDP-User's Guide*; Enraf-Nonius: Delft, The Netherlands, 1983.

We also studied the magnetic hysteresis for MnCu·1H2O. The hysteresis loop at 4.2 K is shown in Figure 10. The remnant magnetization is equal to 6.3×10^3 cm^3 mol^{-1} G, i.e., ~30% of the saturation magnetization (see below), and the coercive field is ~60 G.

The last experiment concerning the magnetization compares the variations of M versus the applied magnetic field for MnCu·5H2O and MnCu·1H2O. The results at 4.2 K are shown in Figure 11. They reveal what follows: (i) The high-field limits are identical for both compounds and equal to $\sim 23.0 \times 10^3$ cm^3 mol^{-1} G. This value agrees with the saturation magnetization M_S expected for a spin $S = S_{Mn} - S_{Cu} = 2$ per MnCu unit. M_S is then given by

$$M_S = Ng\beta S$$

where N is Avogadro's number and β the electronic Bohr magneton. The theoretical value of M_S for $S = 2$ and $g = 2$ is 23.3×10^3 cm^3 mol^{-1} G. (ii) The increase of M versus H is much slower for MnCu·5H2O than for MnCu·1H2O. For instance, half of the saturation magnetization is reached at 7500 G for the former compound and at only 500 G for the latter. (iii) The slope in zero field of the M versus H plot for MnCu·1H2O is extremely large, actually of the order of 2×10^2 cm^3 mol^{-1}. The fact that the zero-field susceptibility $(dM/dH)_{H=0}$ is not infinite is essentially due to the demagnetization field created by the surface of the sample. Moreover, the experiment is carried out with a polycrystalline powder, so that the susceptibility is averaged over all directions, including the hard-magnetization direction.

EPR Spectra

The powder EPR spectra of MnCu·5H2O and MnCu·1H2O exhibit both a single and almost symmetrical band centered at $g = 2.00$, without detectable half-field transition. The line widths, however, are significantly different. At room temperature, they are equal to 327 (4) G for MnCu·5H2O and 104 (4) G for MnCu·1H2O and do not vary significantly versus temperature. It is well established that the line widths of magnetically concentrated systems result from the combined effects of dipolar interactions, which broaden the lines, and exchange interactions, which narrow the lines. In the present case, this latter effect largely dominates when passing from the hydrated to the dehydrated phase. The broad line observed for MnCu·5H2O indicates that the exchange narrowing condition is not obtained. This is consistent with the essentially one-dimensional character of this compounds. In MnCu·1H2O, according to the magnetic susceptibility data, the one-dimensional character is almost completely lost. The problem set is the mechanism of the interchain interactions. In MnCu(pbaOH)(H2O)3, which orders ferromagnetically at 4.6 K, it has been suggested that the dominant interchain interactions were of the exchange nature in one of the directions perpendicular to the chain axis and of the dipolar nature in the other direction.[11] Gatteschi et al. have stated that in the Mn(II)–organic radical-chain compound ordering ferromagnetically at 7.8 K, the dominant interchain interactions were dipolar.[12] It results from this EPR study that the three-dimensional exchange interactions play the key role in the onset of the magnetic ordering for MnCu·1H2O. Let us mention, finally, that we do not detect short-range order effects on the powder sample of MnCu·1H2O.

Discussion and Conclusion

In this last section, we will discuss successively the problem of the structure of the MnCu compounds and then the mechanism of the three-dimensional ordering.

The fact that we have not succeeded in solving the crystal structure of MnCu·5H2O or MnCu·1H2O has been a difficulty in our work. Actually, the slow diffusion processes only give extremely tiny and fragile crystals of MnCu·5H2O. These crystals break under vacuum. The absence of suitable crystals, in the meantime, has offered to us a novel opportunity to test the possibilities of the XANES and EXAFS techniques in the structural area. These techniques allowed us, in particular, to determine without any ambiguity that the geometry around the Mn(II) ion was octahedral for both MnCu·5H2O and MnCu·1H2O. The hypothesis of tetrahedral surroundings in MnCu·1H2O, to which we initially subscribed, may be completely ruled out. Actually, both the Mn(II) and Cu(II) coordination spheres are almost unchanged when passing from the hydrated phase to the dehydrated one, which is quite consistent with the fact that the powder X-ray patterns are almost identical. From a structural viewpoint, the loss of four water molecules only leads to a slight contraction of the lattice. These water molecules are not coordinated to the metals. Moreover, the radius of the coordination sphere around Mn(II) is consistent with Mn–O bonds. In contrast with the previously described MnCu compounds,[11,17,20] MnCu·5H2O and MnCu·1H2O, from a structural viewpoint, are not one-dimensional systems. The units like that shown in Figure 7 pack together through Mn–O apical bonds involving a Mn(II) ion of one unit and two carboxylato oxygen atoms of another one. It is unfortunately not possible to go further into the description of the packing.

Even though the loss of four water molecules does not modify significantly the structure of the MnCu compounds, it dramatically changes the magnetic properties. As a matter of fact, MnCu·5H2O orders antiferromagnetically around 2.3 K, whereas MnCu·1H2O presents a spontaneous magnetization below 14 K. In spite of the three-dimensional packing, the magnetic properties of MnCu·5H2O, except below 4 K, are those expected for an alternating bimetallic chain with oxamido and carboxylato bridges. This apparent paradox may be interpreted as follows: The only magnetic orbital centered on Cu(II) and involved in the Mn(II)–Cu(II) exchange pathways is of the $d_{x^2-y^2}$ type; it is localized in the same plane as the oxamido group on the one hand, and of the carboxylato on the other hand. This magnetic orbital does not overlap with the d_{z^2}-type magnetic orbital centered on Mn(II) and pointing toward the apical oxygen atoms participating to the three-dimensional packing. Moreover, the noncoordinated water molecules prevent the through-space interactions. It follows that, from a magnetic susceptibility viewpoint, MnCu·5H2O essentially behaves as a one-dimensional system. The three-dimensional interactions affect the magnetic properties only in the very low temperature range. This one-dimensional character is much less pronounced in MnCu·1H2O, likely owing to the through-space interactions occurring in the absence of noncoordinated water molecules. The EPR suggests that these interactions are due to exchange rather than to dipolar effects. They lead to a spin structure where all the $S_{Mn} = {}^5/_2$ local spins are aligned along a same direction, the $S_{Cu} = {}^1/_2$ local spins being aligned along the opposite direction. The saturation magnetization perfectly corresponds to a $S = 2$ resulting spin per MnCu unit.

The ferromagnetism versus ferrimagnetism problem maybe deserves a few comments in relation to what we have written in a previous paper[11] dealing with MnCu(pbaOH)(H2O)3. For this compound exhibiting a spontaneous magnetization below 4.6 K, the interchain interactions are much weaker than the intrachain ones, and down to ~10 K, it behaves as a ferrimagnetic chain compound. It was therefore appropriate to describe the magnetic ordering as resulting from ferromagnetic interactions between ferrimagnetic chains. For MnCu·1H2O, in contrast, the one-dimensional character is lost at temperatures as high as 100 K and it is then perhaps preferable to speak of a molecular-based ferrimagnet.

MnCu·1H2O is a fascinating molecular-based material, which is still far from having revealed all its secrets. Its ordering temperature is to our knowledge the highest reported so far for a molecular-based compound with a perfectly defined chemical formula. We are presently trying to shift T_c toward higher temperatures through subtle chemical changes in the coordination spheres of the metal centers.

Acknowledgment. We would like to express our deepest gratitude to the Société Nationale Elf Aquitaine, which has financially supported this work and offered a research grant to K.N. We are also most grateful to A. Michalowicz for providing us his programs to fit the EXAFS data and to J. P. Audière, who performed the thermogravimetric analysis.

Appendix

Let us consider an alternating bimetallic chain:

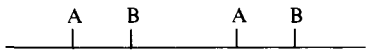

with S_A and S_B local spins, g_A and g_B local g factors, and $J_{AB}(1 + \alpha)$ and $J_{AB}(1 - \alpha)$ interaction parameters between nearest neighbors. S_A is treated as a classical spin and S_B as a quantum spin. One puts

$$J = J_{AB}[S_A(S_A + 1)]^{1/2} \qquad G = g_A[S_A(S_A + 1)]^{1/2}$$

$$g = g_B \qquad s = S_B \qquad x = J/kT$$

The molar magnetic susceptibility is then given by

$$\chi_M = (N\beta^2/3kT)\{g^2[s(s + 1)(1 - P) + 2QR] + 2gG(Q + R) + G^2(1 + P)\}/(1 - P)$$

with

$$P = A_1/A_0$$

$$Q = x[(1 + \alpha)B_0 + (1 - \alpha)B_1]/A_0$$

$$R = x[(1 - \alpha)B_0 + (1 + \alpha)B_1]/A_0$$

and

$$A_0 = (2\pi/\Lambda^2)\sum_{\sigma=-s}^{+s}\sum_{\epsilon=\pm}[\epsilon \exp(\sigma\lambda_\epsilon)/\sigma^2](\sigma\lambda_\epsilon - 1)$$

$$A_1 = (\pi/\Lambda^4)\sum_{\sigma=-s}^{s}\sum_{\epsilon=\pm}[\epsilon \exp(\sigma\lambda_\epsilon)/\sigma^4] \times [\sigma^3\lambda_\epsilon^3 - 3\sigma^2\lambda_\epsilon^2 + (6 - \sigma^2\lambda^2)\sigma\lambda_\epsilon + \sigma^2\lambda^2 - 6]$$

$$B_0 = (2\pi/\Lambda^2)\sum_{\sigma=-s}^{s}\sum_{\epsilon=\pm}\epsilon \exp(\sigma\lambda_\epsilon)$$

$$B_1 = (\pi/\Lambda^4)\sum_{\sigma=-s}^{s}\sum_{\epsilon=\pm}\epsilon \exp(\sigma\lambda_\epsilon)/\sigma^2][\sigma^2\lambda_\epsilon^2 - 2\sigma\lambda_\epsilon + 2 - \sigma^2\lambda^2]$$

λ_+, λ_-, λ^2, and Λ^2 are defined as

$$\lambda_+ = -2x \qquad \lambda_- = \alpha\lambda_+ \qquad \lambda^2 = 2x^2(1 + \alpha^2)$$

$$\Lambda^2 = x^2(1 - \alpha^2)$$

Supplementary Material Available: Tables SVII–SIX giving anisotropic thermal parameters of non-hydrogen atoms, coordinates of hydrogen atoms, and hydrogen bonds for NiCu, Figure S13 giving the experimental and calculated data for the first shell of neighbors at the copper edge, and Figure S14 giving the same information at the manganese edge (5 pages). Ordering information is given on any current masthead page.

Crystal, Molecular Structure, and Magnetic Properties of Bis(tetra-*n*-butylammonium)bis(4-(dicyanomethylene)-1,2-dimercaptocyclopent-1-ene-3,5-dionato-*S*,*S*′)cuprate(II), $[n\text{-Bu}_4N]_2[Cu(dcmdtcroc)_2]$: A Dimer with Weak Ferromagnetic Coupling

N. Venkatalakshmi,[1a] Babu Varghese,[1a] S. Lalitha,[1a] Raymond F. X. Williams,[1b] and P. T. Manoharan*[1a]

Contribution from the Department of Chemistry, Indian Institute of Technology, Madras-600036, India, and Department of Chemistry, Howard University, Washington, D.C. 20059.
Received April 8, 1988

Abstract: An extended dithiolene complex $(n\text{-Bu}_4N)Cu(dcmdtcroc)_2$ has been prepared and characterized by X-ray diffraction and magnetic studies. The crystal structure reveals the anion to be nonplanar and the dihedral angle between the two chelate planes to be 36.76°. The compound crystalizes in the space group *Pbca* with eight molecules per unit cell. The structural parameters are a = 18.087 (7) Å, b = 32.325 (9) Å, c = 18.236 (7) Å, with the intradimer Cu–Cu distance being 4.88 Å. The magnetic susceptibility measurements fitted to the Bleaney–Bower's expression and corrected for molecular field corrections yielded an intradimer ferromagnetic coupling ($2J$ = 12 cm^{-1}) and a very weak interdimer antiferromagnetic coupling (J' = −0.04 cm^{-1}). The powder EPR spectra observed, consistent with the structure and susceptibility findings, show well-resolved triplet spectra at room temperature and a considerable increase in intensity as the temperature is lowered. The spin Hamiltonian parameters have been derived not only from angular variation EPR study of single crystal but also from the computer simulation of polycrystalline EPR spectra at two different frequencies.

The dithiolene complexes of transition-metal ions, $[M(S_2C_2R_2)_2]^{n-}$, where R = H, CN, CF_3, etc. and M = Ni, Cu, Pd, etc., exhibit low-dimensional cooperative phenomena,[2] columnar crystallographic packing,[3] and interesting magnetic properties.[4-8] The variety in stacking and magnetic properties of these metal dithiolene complexes is made possible by their ability to form grossly planar structures irrespective of the metal ion or their oxidation state. Large delocalization of the highest occupied molecular orbitals of π-symmetry is one among the many reasons that promotes columnar stacking, which in turn is responsible for their interesting magnetic properties. In addition, their ability to undergo reversible electron-transfer reactions to yield stable species promotes the formation of donor–acceptor complexes with a variety of organic-based cations. Hence, these systems have

(1) (a) Indian Institute of Technology, Madras, India. (b) Howard University Washington, D. C.
(2) Keller, H. J. *Low Dimensional Cooperative Phenomena*; Plenum: New York, 1975.
(3) Manoharan, P. T.; Noordik, J. H.; de Boer, E.; Keijzers, C. P. *J. Chem. Phys.* **1981**, *74*, 1980–1989.
(4) Kuppusamy, P.; Ramakrishna, B. L.; Manoharan, P. T. *Proc. Indian Acad. Sci.* **1984**, *93*, 977–1001.
(5) Plumlee, K. W.; Hoffmann, B. M.; Ibers, J. A.; Soos, Z. G. *J. Chem. Phys.* **1975**, *63*, 1926–1942.
(6) Plumlee, K. W.; Hoffmann, B. M.; Ratajack, M. T.; Kannewurf, C. R. *Solid State Commun.* **1974**, *15*, 1651–1654.
(7) Isett, L. C.; Rosso, D. M.; Bottger, G. L. *Phys. Rev.* **1980**, *B22*, 4739–4743.
(8) Ramakrishna, B. L.; Manoharan, P. T. *Inorg. Chem.* **1983**, *22*, 2113–2123.

0002-7863/89/1511-5748$01.50/0 © 1989 American Chemical Society